**Proceedings of the ASME 2017 International Design Engineering Technical Conferences and Computers and Information in Engineering Conference**
**IDETC/CIE 2017**
**August 6-9, 2017, Cleveland, Ohio, USA**

**DETC2017-68149**

# TOWARDS COMPUTATIONAL SYNTHESIS OF MICROSTRUCTURAL CRYSTALLINE MORPHOLOGIES FOR ADDITIVE MANUFACTURING APPLICATIONS

**John G. Michopoulos, Athanasios P. Iliopoulos**
**John C. Steuben, Andrew J. Birnbaum**
Computational Multiphysics Systems Laboratory
Center of Materials Physics and Technology
Naval Research Laboratory
Washington DC, 20375, USA

**Yao Fu**
Dept. of Aerospace Engineering and Engineering Mechanics
University of Cincinnati
Cincinnati, OH 45221

**Jeong-Hoon Song**
Faculty, Materials Science and Engineering Program
Dept. of Civil, Environmental, and Architectural Engineering
University of Colorado
Boulder, CO 80309

## ABSTRACT

*Powder-based additive manufacturing technologies introduce severe variations in microstructure in terms of grain size and aspect ratio that, coupled with porosity, can result in dramatic effects on the functional (mechanical, thermal, fatigue, fracture etc.) performance of as-produced parts. In the context of Integrated Computational Materials Engineering (ICME), it is essential develop a computationally efficient approach for generating synthetic microstructural morphologies that reflect these process-induced features. In the present paper, we employ two methodologies for computing the evolution of metal solidification at the microstructural level as a function of process parameters associated with additive manufacturing. The first method is the Continuum Diffuse Interface Model (CDM) applied to an arbitrary material system, and the second, the Multi-Phase Field Model (MPFM) applied to pure nickel (Ni). We present examples of microstructures generated by these methods within the context of additive manufacturing.*

## INTRODUCTION

The paradigm of Integrated Computational Materials Engineering (ICME) has been proposed as a viable and effective approach for the control of manufacturing processes including additive manufacturing by various research organizations and investigators [1–4]. In our view, ICME is essential for controlling additive manufacturing processes in a manner that enables the discovery of how process parameters determine material properties via the interdependence of the micro-, meso-, and macro-structure. It also has the potential to enable the control of AM processes for tailoring the features at each of these scales, including microstructure. In Fig. 1 we present the entities involved in an ICME framework as we envision it.

The goal motivating the creation of an ICME framework, is the desire to be able to control the AM process parameters such that the functional performance of the manufactured part satis-

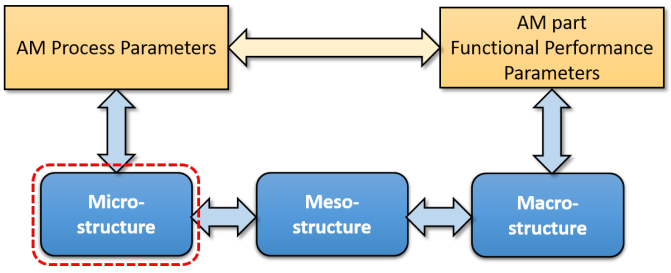


**FIGURE 1**: Entities involved in proposed ICME framework for Additive Manufacturing.


Copyright © 2017 ASME
This work was authored in part by a U.S. Government employee in the scope of his/her employment.
ASME disclaims all interest in the U.S. Government's contribution.
**Downloaded From: http://proceedings.asmedigitalcollection.asme.org/ on 11/07/2017 Terms of Use: http://www.asme.org/about-asme/terms-of-use**

fies specific performance requirements. Ideally, such a framework would allow the prediction of the functional performance of a part once the process parameters are known (left to right transition in Fig. 1); Conversely, it would enable controlling the process parameters to tailor the process for a desired functional performance (right to left). However, the actual physical mechanisms controlling this desirable functional relationship between process and functional performance can only be realized via the compositional aggregation of sub-processes present at each of the micro-, meso- and macro- length scales. The recognition of the fact that the AM processes have a direct impact on the morphological characteristics of the microstructure is hardly disputable as it can be evidenced by a plethora of studies for various material systems and processes as indicated in [5–8]. Less prevalent, but still applicable, are the effects of the process parameters on the mesoscale either through the microscale, or, via direct influence from the process. Remelting and resolidification fronts, anisotropic banding and porosity are process induced features that fall in to this category. Finally, the effect of the process parameters through the interaction of the mesoscopic and microsopic features, or those directly associated with the macroscale, like extreme size porosity, warping and surface finish, must also be considered. In our proposed ICME framework, all the invertible arrows between the blocks in Fig. 1, represent relations and associated computational functionality that need to be encapsulated in a manner that preserves the relationship between successive representations of matter at distinct length scales. Creating the modeling and simulation infrastructure that permits the construction of this synthetic representation of material at all these length scales constitutes our long term goal. The motivation for this goal is the need for the ability to tailor the AM process of interest for specified functional outcomes that satisfy performance requirements.

Being able to connect all features observed at various length scales would enable the transitive closure of the functional morphisms in Fig. 1. The relationship that needs to be established first is the one closest to the AM-process and expresses the relationship between the process parameters and the features of the microstructure. Within the scope of a new grand-challenge project for establishing the scientific principles of layered deposition processes for novel naval materials, recently initiated at the Naval Research Laboratory (NRL), we have identified a grain size variation of 3 to 4 orders of magnitude, and aspect ratios that span 2-3 orders of magnitude [9]. These variations are in addition to multiscale porosities that appear as well, all as a result of the chosen process parameters. It is therefore imperative that any computational infrastructure aligned with the ICME paradigm for AM processes, has the ability to create computationally synthetic microstructures that exhibit these features. The specific objective of the present work is to explore potential methods that can be utilized to predict and simulate evolution of microstructure in a manner that accounts for such features.

In the following section we will describe a brief overview of methods that are capable of modeling solidification of liquid metals and alloys as it evolves from nucleation centers in a volume and converges to a particular crystalline microstructure morphology. After this section we describe the continuous diffuse interface model (CDM) method and then the multi phase field model (MPFM) method, followed by a section on the material properties used for this method. We subsequently provide some examples of creating synthetic microstructures by each of the methods and after their discussion our conclusions and plans complete the present work.

## FIELD THEORIES OF MOVING BOUNDARIES

A careful observation of the area involving theories of moving boundaries between phases, easily yields the realization that there are two approaches for phase-field modeling as noted in [10]. One class of approaches is only concerned with reproducing the sharp-interfaces between phases, while the other class of approaches use thermodynamic treatment with gradient flow to account for the evolution of the sharp boundaries between phases in physics informed manner.

In order to support the present study for generating synthetic microstructures for Random Volume Elements (RVEs), we have established a computational infrastructure that implements a CDM for simulating grain evolution within 3D domains and falls within the first category of methods that are interested for the interfacial evolution alone. It was first introduced in [11] for 2D domains and without grain aspect ratio control capability. In the present case we generalized this model for 3D domains and introduced the proper parameters for controlling the size and aspect ratio variation distributions.

When it comes to the second category of methods, the development of continuous field theories for moving boundaries such as solidification began with the diffusive interface model more than a century ago [12] followed by the development of the phase field model (PFM) by Cahn and Hilliard [13] and more recently by [14].

PFM approaches are widely used in science and engineering to model a variety of moving interface phenomena. Typical examples are the dendritic alloy solidification [15], various moving boundary phenomena including solidification and microstructure evolution in materials processing [10, 16–20], fracture problems [21, 22] and multiscale up-scaling for nonlinear materials [23].

The advantage of the PFM lies on its capability to address the numerical problem of tracking a sharp solid-liquid interface without rigorous attention to the involved physics. Its principal characteristic is the diffuse interface between two phases, described by a steep but continuous transition of a phase field variable between two states. The PFM models are also benefited by the fact that they are derived in a thermodynamically consistent


Copyright © 2017 ASME

Downloaded From: http://proceedings.asmedigitalcollection.asme.org/ on 11/07/2017 Terms of Use: http://www.asme.org/about-asme/terms-of-use

manner which enables the correlation of the model parameters with proper thermodynamic variables. Subsequently, the multi-phase field model (MPFM) was developed [24–26] to address an arbitrary number of different distinct phases or grains of different orientation. In the MPFM approach, a grain $\alpha$ can be distinguishable from other grains either by its orientation or phase (or both) and is endowed with an individual phase field variable $\phi_\alpha$.

Despite the significant advances in MPFM, a major difficulty in its wide applicability to real multicomponent alloy systems is the lack of knowledge of several required materials-specific parameters, such as bulk free energies, the diffusion coefficients, interfacial free energy, kinetic coefficients and so forth. To supplement experimental measurements, or to generate some of these quantities when experiments are not feasible, computational techniques have become essential tools for extracting the relevant material parameters [27–31]. For example, the small anisotropy coefficient that is vital to determining the shape and velocity of dendritic growth cannot be measured accurately by existing experimental techniques. Instead, *ab initio* molecular dynamics (MD) simulations have been shown to be capable of computing the necessary phase field parameters and their associated small anisotropies. The semi-empirical embedded atom model (EAM) potentials have been introduced to compute the kinetic and diffusion coefficient of a variety of pure metals including Cu, Ni, Au and Ag [28, 30]. Several investigators employed an analysis of the equilibrium fluctuation spectrum of the solid-liquid boundary to extract the interfacial free energy and its small anisotropy in Ni, Cu, Fe, and Al metals [27–29, 32].

An important question relating to the applicability of PFM and MPFM is whether these methods, in which the relaxation dynamics are driven by thermodynamic forces, can capture well the physical phenomena at the time and length scale achievable by atomistic models. In other words, whether the PFM and atomistic simulation such as MD can be equivalent in describing nano-scale phenomena. A comparison of the results from PFM and MD simulations of the propagation of the planar solidification front of a two-phase $Ni_xZr_{1-x}$ crystal-liquid sample subjected to an abrupt temperature drop has been demonstrated in [33, 34]. They have also shown that the MD and PFM approaches can yield equivalent results in a manner that enables key physical parameters to be transferable from the former method to the latter one. In particular, the free energy density participating in the formulation of the PFM guided by the free energy in the atomistic calculations was found to be the enabling factor in bridging the gap between the two approaches [34]. Recently, we have also demonstrated the ability to bridge MD with MPFM for a Nickel (Ni) system by calibrating the MPFM to a MD-based analysis [35]. In fact, many critical thermodynamic and kinetic parameters were calibrated in this study using MD for the solidification process of Ni at moderate undercooling degree ($\sim$200 K) and the equivalence of MD and PFM methods was demonstrated at the nanometer length scales.

## BRIEF REVIEW OF THE CONTINUUM DIFFUSE INTERFACE MODEL

In the CDM, an arbitrary polycrystalline microstructure is described by a set of continuous field variables $\eta_i$ $(i = 1, ..., p)$, that are called orientation field variables for distinguishing different orientations of grains and $p$ is the number of possible grain orientations.

It is assumed that across the grain boundaries between the grain $\eta_1$ and its neighbors the value of $\eta_1$ changes continuously from 1 to 0. We now can express the total free energy of an inhomogeneous system in terms of all the orientation field variables and their gradients as:

$$F = \int [f_0(\eta_1(r), \eta_2(r), ..., \eta_p(r)) + \sum_{i=n}^{p} \frac{\kappa_i}{2} (\nabla \eta_i(r))^2] d^3r, \quad (1)$$

where $f_0$ is the local free energy density, which is a function of field variables $\eta_i$, and $\kappa_i$ are the gradient energy coefficients. The main requirement for $f_0$ is that it has $p$ degenerate minima with equal depth, $f_{min}$ , located at $(\eta_1(r), \eta_2(r), ..., \eta_p(r)) = (1, 0, ..., 0), (0, 1, ..., 0), ..., (0, 0, ..., 1)$ in $p$-dimensional space.

Because the orientation field variables are non-conserved quantities, their local evolution rates can be considered linearly proportional to the variational derivative of the total free energy with respect to the local orientation field variable and therefore they are governed by the Ginzburg–Landau equations,

$$\frac{\partial \eta(r,t)}{\partial t} = -L \frac{\delta F}{\delta \eta(r,t)}, \; i = 1, 2, ..., p, \quad (2)$$

where $L$ are relaxation coefficients, $t$ is time, and $F$ is total free energy. Substitution of the free energy form in Eq. 1 into this equation leads to the form:

$$\frac{\partial \eta(r,t)}{\partial t} = -L[\frac{\delta f_0(\eta)}{\eta} - \kappa \nabla^2 \eta]. \quad (3)$$

By following the process described in [11] in specializing the initial free energy we can finally derive the system of equations that need to be solved for obtaining the evolutions of all $\eta_i$ in the form

$$\frac{\partial \eta_i}{\partial t} = -L_i[-a_1 \eta_i + a_2 \eta_i^3 + 2a_3 \eta_i \sum_{j \neq i}^{p} \eta_j^2 - \kappa_i \nabla^2 \eta_i], \quad (4)$$

for $i = 1, 2, ..., p$ and for $a_k, (k = 1, 2, 3)$ defined as indicated in [11] to have the values $a_1 = a_2 = 1$, $a_3 = a_1/2$.

To simulate the grain growth evolution for the purpose of generating synthetic RVE microstructures, the set of equations (4) are solved numerically by discretizing them in space and time. The Laplacian is discretized by the following finite dif-


Copyright © 2017 ASME

Downloaded From: http://proceedings.asmedigitalcollection.asme.org/ on 11/07/2017 Terms of Use: http://www.asme.org/about-asme/terms-of-use

ference discrete form,

$$\nabla^2\eta_i = \frac{1}{3(\Delta h)^2}\left[\tau\left(\eta_i(x-\Delta h,y,z)+\eta_i(x+\Delta h,y,z)+\right.\right.$$
$$+\eta_i(x,y-\Delta h,z)+\eta_i(x,y+\Delta h,z)-\eta_i(x,y,z)\Big)+, \quad (5)$$
$$\left.+\eta_i(x,y,z-\Delta h)+\eta_i(x,y,z+\Delta h)\right]$$

where $\Delta h$ is the size of the grid element and $\tau$ represents a bias factor on the $x-y$ plane such that we can tune a desired variation of grain aspect ratio. In fact, if we consider that the energy gradient coefficients $\kappa_i$ are not represented by scalar quantities (isotropic case), but rather they are second order diagonal tensors $\boldsymbol{\kappa}_i$ (anisotropic case), then this factor can be thought of as the proportion of discrepancy of the gradient energy coefficients along directions $x$ and $y$ relative to those along $z$. This generalization can be expressed by $\boldsymbol{\kappa}_i = ((\tau_x\kappa_i,0,0),(0,\tau_y\kappa_i,0),(0,0,\kappa_i))$. For the case where we want to allow the response to be the same on both directions in the $x-y$ plane we have $\tau=\tau_x=\tau_y$, and this is the case that we will use for our numerical analysis later in this paper.

The discretization with respect to time was implemented via a simple explicit forward Euler scheme described by,

$$\eta_i(t+\Delta t) = \eta_i(t) + \frac{d\eta_i}{dt}\Delta t, \quad (6)$$

where $\Delta t$ represents the integration time step. Thus, for a given initial distribution of $\eta_i$, which describes the initial grain structure, the temporal and spatial evolution of the microstructure can be obtained by solving equation (4) numerically via Eqs. (5) and (6).

## BRIEF REVIEW OF THE MULTI-PHASE FIELD MODEL

The multigrain growth model adopted here is based on the conventional MPF developed in [24–26]. The general free energy functional $F$, incorporates multiple physical phenomena including contributions from interfacial $f^{int}$ and chemical $f^{chem}$ energy densities as expressed:

$$F = \int_\Omega f^{int} + f^{chem} \quad (7)$$

where the interfacial energy density is defined by

$$f^{int} = \sum_{\alpha,\beta=1,\alpha\neq\beta}^{N} \frac{4\sigma_{\alpha\beta}}{\eta_{\alpha\beta}}\left\{-\frac{\eta_{\alpha\beta}^2}{\pi^2}\nabla\phi_\alpha\cdot\nabla\phi_\beta+\phi_\alpha\phi_\beta\right\}, \quad (8)$$

and the chemical energy density $f^{chem}$ is defined for a pure system containing only one element according to

$$f^{chem} = \sum_{\alpha=1,..,N} h(\phi_\alpha) f_\alpha \quad (9)$$

In Eqs. (7)-(9), $\phi_\alpha$ ($\alpha$=1 ,..., $N$) is the phase field variable (i.e. order parameter) which represents a grain $\alpha$ with a different orientation; $N$ represents the total number of grains in the system, and $\phi_\alpha$=1 indicates that the grain $\alpha$ is present (i.e. the solid phase) while $\phi_\alpha$=0 indicates its absence (i.e. the liquid phase). $\sigma_{\alpha\beta}$ the interfacial energy between phases (or grains) $\alpha$ and $\beta$, $\eta_{\alpha\beta}$ the interface width that is assumed to be constant $\eta$ for all interfaces, $f_\alpha$ is the bulk free energy of an individual phase (grain) $\alpha$, and $h(\phi_\alpha)$ represents a contour function. The condition $\sum_{\alpha=1}^{N}\phi_\alpha(x)=1$ must be satisfied at all time instances at any spatial position $x$ within the domain.

The evolution of grain $\alpha$ can be considered as $\dot{\phi}_\alpha = -\sum_{\beta=1}^{N}\frac{\pi^2}{8m\eta}\mu_{\alpha\beta}\left(\frac{\delta F}{\delta\phi_\alpha}-\frac{\delta F}{\delta\phi_\beta}\right)$, and therefore through Eqs. (8)-(9) we can obtain

$$\dot{\phi}_\alpha = \sum_{\beta=1}^{N}\frac{\mu_{\alpha\beta}}{m}\left\{\sum_{\gamma=1}^{N}\left(\sigma_{\beta\gamma}-\sigma_{\alpha\gamma}\right)I_\gamma+\frac{\pi^2}{8\eta}h'\Delta g_{\alpha\beta}\right\} \quad (10)$$

$$I_\gamma = \nabla^2\phi_\gamma + \frac{\pi^2}{\eta^2}\phi_\gamma \quad (11)$$

where $\mu_{\alpha\beta}$ stands for the interfacial mobility at the boundary of grains $\alpha$ and $\beta$, $m$ represents the total number of locally existing grains at the spatial point, and $\Delta g_{\alpha\beta}$ is the free energy difference between grains $\alpha$ and $\beta$.

However, due to the difficulty of identifying a suitable contour function for the case of multiple junctions, a so-called antisymmetric approximation is further introduced [9]. Applying antisymmetric approximation to Eqs. (10) and (11) yields the final form of grain evolution law which is adopted in the current study:

$$\dot{\phi}_\alpha = \sum_{\beta=1}^{N}\mu_{\alpha\beta}\left\{\sigma_{\alpha\beta}\left(\phi_\beta\nabla^2\phi_\alpha-\phi_\alpha\nabla^2\phi_\beta\right.\right.$$
$$\left.\left.+\frac{\pi^2}{2\eta^2}\left(\phi_\alpha-\phi_\beta\right)\right)+\frac{\pi}{\eta}\sqrt{\phi_\alpha\phi_\beta}\Delta g_{\alpha\beta}\right\}. \quad (12)$$

## DISCRETIZATION OF THE MULTI-PHASE FIELD MODEL

The particle difference method (PDM) [36–38] is used for implementing the discrete form of the MPFM analysis. The PDM has shown great flexibility in discretizing various types of partial differential equations (PDEs) while also can reach identical


Copyright © 2017 ASME

Downloaded From: http://proceedings.asmedigitalcollection.asme.org/ on 11/07/2017 Terms of Use: http://www.asme.org/about-asme/terms-of-use

results as the finite difference method (FDM), which has been frequently been used to solve phase field model by the material science community.

The PDM possesses desirable features required for the numerical method. It easily handles the high-order derivatives of the functional, and it relies on the neighboring nodes within a dilation parameter suitable for local refinement and dynamic adaptivity. This PDM has the advantages as other mesh-free methods, i.e., the grid can be easily adapted to resolve the sharp features of the solution fields. Additionally, it does not require numerical integration as it does not involve a weak formulation and gives higher rates of convergence than other weak form based methods. Furthermore, the computational speed for computing the derivatives of mesh-free approximation can be accelerated by the derivative-approximating technique. The PDM has been shown to be highly robust, accurate and very easy to implement compared to other mesh-free methods.

The PDM is a point collocation method that obtains shape functions and the approximated differential coefficient vector at the nodes based on the moving least-square approximations. Therefore, the partial differential equations can be directly written into discrete forms in terms of the approximated differential coefficient vector in the PDM, without the weak form formulation. While the details of this method can be found in our previous work [36–38], the differential coefficient vector up to the $1^{st}$ order, $\mathbf{D}^{\alpha}_{\mathbf{x}}u(\mathbf{x})$, of a continuous function $u(\mathbf{x})$, in 3-D is briefly given as follows:

$$\mathbf{D}^{\alpha}_{\mathbf{x}}u(\mathbf{x}) = \left[ u(x_1,x_2,x_3)\, \frac{\partial u(x_1,x_2,x_3)}{\partial x_1}\, \frac{\partial u(x_1,x_2,x_3)}{\partial x_2}\, \frac{\partial u(x_1,x_2,x_3)}{\partial x_3} \right] \quad (13)$$

and can be obtained by $\mathbf{D}^{\alpha}_{\mathbf{x}}u(\mathbf{x}) = \mathbf{M}^{-1}(\mathbf{x})\mathbf{B}(\mathbf{x})\mathbf{u} = \sum_I^N \Phi^{\alpha}_I u_I$ with

$$\mathbf{M}(\mathbf{x}) = \sum_{I=1}^{N} \omega\left(\frac{\mathbf{x}_I - \mathbf{x}}{\rho_{\mathbf{x}}}\right) \begin{bmatrix} 1 & d_{I1} & d_{I2} & d_{I3} \\ & d_{I1}^2 & d_{I1}d_{I2} & d_{I1}d_{I3} \\ & & d_{I2}^2 & d_{I2}d_{I3} \\ sym. & & & d_{I3}^2 \end{bmatrix} \quad (14)$$

where $u_I$ is the nodal solution at discrete nodes at position $\mathbf{x}_I$($I$=1, …, $N$), and $d_{Ii} = x_{Ii} - x_i$. $\rho_x$ is the dilation function indicating the radius of the weight function $\omega\left((x_I - x)/\rho_x\right)$ and determines the size of the neighborhood of $\mathbf{x}$.

In this study, for the spatial discretization of the governing equation (i.e. the MPF model in Eq. (12)), we consider a computational domain that is spatially discretized by distributing nodes in the interior domain and on the boundaries. The PDM can be directly applied to compute the differential forms of governing equations at these distributed nodes. Besides from the spatial discretization, applying the explicit time integration scheme to Eq. (12) yields

$$\begin{aligned} \frac{\phi_\alpha^{n+1} - \phi_\alpha^n}{\Delta t} = \sum_{\beta=1}^{N} \mu_{\alpha\beta} \Bigg\{ \sigma_{\alpha\beta} \Bigg( & \phi_\beta^n \nabla^2 \phi_\alpha^n - \phi_\alpha^n \nabla^2 \phi_\beta^n \\ & + \frac{\pi^2}{2\eta^2}\left(\phi_\alpha^n - \phi_\beta^n\right)\Bigg) + \frac{\pi}{\eta}\sqrt{\phi_\alpha^n \phi_\beta^n}\,\Delta g_{\alpha\beta} \Bigg\} \end{aligned} \quad (15)$$

where $\Delta t$ is the time step and the superscript on the phase field $\phi$ represents the index for the time step. By discretizing Eq. (15) with the PDM, the discretized governing equation can be written as

$$\sum_{I=1}^{N} L_I^{\Omega}(\mathbf{x})\phi_{\alpha I}^{n+1} = F_\phi^{\Omega}(\mathbf{x}) \quad (16)$$

where the subscript $I$ denotes the nodal index of the distributed node for the spatial discretization. In Eq. (16), the discrete operator $L_I^{\Omega}(x)$ is given by

$$L_I^{\Omega}(x) = \Phi_I^{(0,0,0)}(x). \quad (17)$$

On the other hand, the generalized force $F_\phi^{\Omega}(x)$ on the right-hand side of Eq. (16) can be written as

$$\begin{aligned} & F_\phi^{\Omega}(\mathbf{x}) = \sum_{I=1}^{N} \Phi_I^{(0,0,0)}(\mathbf{x})\phi_{\alpha I}^n + \\ & + \Delta t \sum_{\beta=1,\ldots,N} \mu_{\alpha\beta} \Bigg\{ \sigma_{\alpha\beta} \Bigg( \Bigg( \sum_{I=1}^{N} \Phi_I^{(0,0,0)}(\mathbf{x})\phi_{\beta I}^n \Bigg) \\ & \sum_{I=1}^{N} \left( \Phi_I^{(2,0,0)}(\mathbf{x}) + \Phi_I^{(0,2,0)}(\mathbf{x}) + \Phi_I^{(0,0,2)}(\mathbf{x}) \right) \phi_{\alpha I}^n - \\ & - \Bigg( \sum_{I=1}^{N} \Phi_I^{(0,0,0)}(\mathbf{x})\phi_{\alpha I}^n \Bigg) \\ & \sum_{I=1}^{N} \left( \Phi_I^{(2,0,0)}(\mathbf{x}) + \Phi_I^{(0,2,0)}(\mathbf{x}) + \Phi_I^{(0,0,2)}(\mathbf{x}) \right) \phi_{\beta I}^n \\ & + \frac{\pi^2}{2\eta^2} \sum_{I=1}^{N} \Phi_I^{(0,0,0)}(\mathbf{x}) \left( \phi_{\alpha I}^n - \phi_{\beta I}^n \right) \Bigg) + \\ & + \frac{\pi}{\eta} \sqrt{\sum_{I=1}^{N} \Phi_I^{(0,0,0)}(\mathbf{x}) \left( \phi_{\alpha I}^n \phi_{\beta I}^n \right)}\, \Delta g_{\alpha\beta} \Bigg\} \end{aligned} \quad (18)$$

in terms of the computed differential operators by the PDM. Comprehensive discussion about the PDM can be found in literature [31-33]; the application of the PDM to coupled MPF and energy balance equations for multi-grain solidification analysis will be presented in future work.

## MATERIALS PARAMETERS IN THE MULTI PHASE FIELD MODEL

The materials parameters needed for the MPF model include the interfacial mobility $\mu$, the interfacial energy $\sigma$, the free energy difference between phases $\Delta g$ , and the interface width $\eta$ be-


Copyright © 2017 ASME

Downloaded From: http://proceedings.asmedigitalcollection.asme.org/ on 11/07/2017 Terms of Use: http://www.asme.org/about-asme/terms-of-use

tween solid and liquid phases. Because the solidification problem is mainly investigated before the complete liquid-to-solid transformation here, the interfacial mobility, interfacial energy, and the interface width among grains in solid phase with different random orientations are not calibrated and are assumed to be the same as the respective quantities for the case of the solid-liquid interface. Since the Ni system has been relatively well investigated, most of the materials parameters are readily available. The kinetic coefficient $\mu*$ (i.e., the constant of proportionality between the velocity of crystallization and the degree of undercooling) [27] and the solid-liquid interfacial free energy ($\gamma$) have been investigated thoroughly by MD techniques because of the difficulty in obtaining their small anisotropy through experimental techniques [27, 29, 35].

The interfacial free energy $\sigma_{\alpha\beta}(\widehat{\mathbf{n}})$ of a weakly anisotropic crystal ( $\widehat{\mathbf{n}}$ is the interfacial normal of the grain $\alpha$) can be expanded in terms of "Kubic harmonics", which is a linear combination of spherical harmonics that obey a cubic symmetry [39]:

$$\begin{aligned}\frac{\sigma_{\alpha\beta}(\widehat{\mathbf{n}})}{\gamma_0} =& 1-3\zeta+4\zeta(n_x^4+n_y^4+n_z^4)+ \\ &+\delta(n_x^6+n_y^6+n_z^6+30n_x^2n_y^2n_z^2)\end{aligned} \tag{19}$$

The anisotropic coefficients $\gamma_0$, $\varsigma$, and $\delta$ have been determined through MD simulation (by employing the EAM interatomic potential) in [35] to be $\gamma_0$=325.88E-3 J/m$^2$, $\varsigma$=0.02269, and $\delta$=-0.01168.

The kinetic coefficient $\mu^*$ can also be written in a format according to the cubic symmetry [25, 26]:

$$\begin{aligned}\mu^*(\hat{n})/\mu_0^* = 1-3\varepsilon+4\varepsilon\left(n_x^4+n_y^4+n_z^4\right) \\ +\kappa\left(n_x^6+n_y^6+n_z^6+30n_x^2n_y^2n_z^2\right)\end{aligned} \tag{20}$$

The $\mu*$ obtained for Ni employing EAM potentials in MD simulations [35] are $\mu^*_{100}$=35.8±2.2, $\mu^*_{110}$=25.5±1.6, and $\mu^*_{111}$=24.1±4.0 in the units of cm/(s K) [21]. Using these results to fit the above equation, we can obtain $\mu^*_0$=31.2 cm/(sK), $\varepsilon$=0.1488, and $\kappa$=0.069. The solution of the MPF method to the 1-D solidification problem predicts a diffusive interface boundary that varies from the solid to the liquid phases as a smooth sine function proceeding to the liquid phase at the velocity $\mu\Delta g$. Thus $\mu$ can be related to $\mu*$ by

$$\mu = \mu * \frac{T_M}{L} \tag{21}$$

The free energy difference between the solid and liquid phases can be estimated as in [10] according to

$$\begin{aligned}\Delta g &= \frac{L(T_M-T)}{T_M} \\ &= \frac{L\Delta T}{T_M}\end{aligned} \tag{22}$$

where $L$ is the latent heat, $T_M$ the melting temperature. For Ni, $L$=2.311E9 J/m$^3$ [27] and $T_M$=1710 K [21].

Another physical parameter required to be determined is the interfacial width between the solid and liquid phases. The crystal-melt interface can extend over several lattice constants. To track the growth process and obtain the interface width, a first step is to distinguish the crystals from the undercooled liquids. We have employed the averaged local bond order parameters proposed by Dellago *et al.* [28], because this approach represents an improved form of the bond orientational order method by Steinhardt *et al.* [29], and they are defined as

$$q_l(i) = \sqrt{\frac{4\pi}{2l+1}\sum_{m=-l}^{l}|q_{lm}(i)|^2} \tag{23}$$

where the complex vector $q_{lm}(i)$ of particle $i$ is expressed by

$$q_{lm}(i) = \frac{1}{N_b(i)}\sum_{j=1}^{N_b(i)} Y_{lm}(r_{ij}). \tag{24}$$

Here, $N_b(i)$ is the number of nearest neighbors of particle $i$, $l$ is a free integer parameter, and $m$ is an integer that runs from $m$=-$l$ to $m$=+$l$, the functions $Y_{lm}(\mathbf{r}_{ij})$ are the spherical harmonics and $\mathbf{r}_{ij}$ is the vector originating from particle $i$ and ending to particle $j$. Depending on the choice of $l$, these parameters are sensitive to different crystal symmetries. $q_6$ is used here as it is good at distinguishing among liquid and different types of crystalline structures.

A further improvement of the above-mentioned method is also introduced later [40] where the following averaged form of the local bond order parameters were introduced:

$$\bar{q}_l(i) = \sqrt{\frac{4\pi}{2l+1}\sum_{m=-l}^{l}|\bar{q}_{lm}(i)|^2} \tag{25}$$

where

$$\bar{q}_{lm}(i) = \frac{1}{\tilde{N}_b(i)}\sum_{k=0}^{\tilde{N}_b(i)} q_{lm}(k) \tag{26}$$

Here the sum from $k$=0 to $\tilde{N}_b(i)$ runs over all neighbors of particle $i$ plus the particle $i$ itself, i.e., the local orientational order vectors $q_{lm}(i)$ is averaged over particle $i$ and its surroundings. Because this averaged local bond order approach has been shown to pro-


Copyright © 2017 ASME

Downloaded From: http://proceedings.asmedigitalcollection.asme.org/ on 11/07/2017 Terms of Use: http://www.asme.org/about-asme/terms-of-use

vide improved accuracy with which different crystal structures can be identified, it was adopted in our study.

The MD results after initial equilibration are processed using the averaged local bond order method to obtain the $\overline{q}_6$ for each atom, which is subsequently averaged over equal-sized bins and scaled to the range of (0∼1) in order to provide initial phase field conditions to the PFM model. To reduce the possible uncertainties introduced by the temperature, ten parallel simulations are conducted for each example and averaged to provide for the initial PFM condition and to generate the evolution snapshots during the solidification process. The typical values of $\overline{q}_6$ are 0.40 and 0.15 in the crystal and liquid phases, respectively, around the melting temperature $T_M$. According to the equilibrium state solution to the MPF model of two phase interface $\phi_{eq}(x) = \frac{1}{2}\left(1 - \sin\frac{\pi}{\eta}x\right)$ [41], a fitting of the MD results to the equilibrium solution yields $\eta$=12-16 Å and this led $\eta$ to be set to 14 Å throughout the PFM simulation.

## REPRESENTATIVE NUMERICAL EXPERIMENTS

To demonstrate the ability to capture the feature of variability of aspect ratio we implemented the CDM presented earlier for an RVE discretized by $512 \times 512 \times 512$ discrete elements. Figure 2 shows the effect of transitioning from an isotropic configuration for the bias coefficient defined in Eq. (5) $\tau = 1$ to an anisotropic configuration for $\tau = 6$ and for an even more acute aspect ratio for $\tau = 12$. All three cases have been computed over the same cloud of randomly distributed solidification nucleation points in the volume of the RVE. The computational implementation of this method was integrated in Matlab using a parallelized kernel programmed in C++. The execution of 1800 steps of the 2.68 Billion DOFs Finite Difference model was completed in 1.7 hours on a 24 core Intel E5 Shared Memory computer.

The variability on the grain size can be trivially achieved by the extend of the period that over which the time integrator evolves. A demonstration of the MPFM approach for Ni grain solidification is shown in Fig. 3 for distinct time instances. This simulation has been performed assuming a homogeneous temperature field and therefore it does not exhibit any anisotropy.

The MPF analysis was conducted with a custom parallelized PDM code. The computational parameters were chosen as follows: the grid size $\Delta x = \Delta y = \Delta z = 2\ \mathring{A}$ to ensure a satisfactory resolution of the interface width. For the time integration of the PFM with the PDM approach, we adopted forward Euler scheme which is conditionally stable. According to our numerical experiments, the PDM retains its numerical stability with the full CFL condition $\Delta t > 1\ fs$, but to make an easy comparison with MD results, we used $\Delta t = 1\ fs$ as the size of stable time integration in our computations. The number of grid points depends on the equilibrated dimension of the simulation cells in the corresponding MD simulation as described in [35]. To reduce the required computational memory, of the MPF analysis, only the nonzero MPF variables are stored in terms of the sparse matrix representation [42].

## CONCLUSIONS AND PLANS

We have introduced two methods for generating synthetic micro structures with controlled morphological characteristics in order to support our ICME paradigm for powder based additive manufacturing processes. We generalized the original 2D version of the CDM in 3D and introduced a bias factor to control the aspect ratio anisotropy of the microstructural grain morphology. We also provided an overview of the MPFM/PFM approach and introduced the PDM as an alternative solution method. We also demonstrated that we can generate synthetic microstructures for an arbitrary material with tailorable grain aspect ratio variability, as well as Ni solidification microstructures, by using the MPFM.

Our plans include adding tailorable porosity morphologies to both methods and implementing temperature gradient boundary conditions for the MPFM in order to drive aspect ratio variability to appear naturally. We also plan to extend the MPFM for multi-component alloy systems. Finally, we plan to connect the morphological characteristics from all scales to crystal plasticity models in order to establish a capability for predicting the mechanical properties of the relevant materials systems. Our initial efforts on this topic can be found in [43].

## ACKNOWLEDGMENT

The authors acknowledge support for this work by the Office of Naval Research through the Naval Research Laboratory's core funding.

## REFERENCES

[1] Council, N. R., 2008. *Integrated Computational Materials Engineering: A Transformational Discipline for Improved Competitiveness and National Security*. The National Academies Press, Washington, DC.

[2] Christodoulou, J., 2012. "ICME-a revolution in materials research culture.". In 53rd AIAA/ASME/ASCE/AHS/ASC Structures, Structural Dynamics and Materials Conference 20th AIAA/ASME/AHS Adaptive Structures Conference 14th AIAA.

[3] Mullins, W. M., and Christodoulou, J., 2013. "ICME - application of the revolution to titanium structures". In 54th AIAA/ASME/ASCE/AHS/ASC Structures, Structural Dynamics, and Materials Conference. Boston, Massachusetts., pp. AIAA 2013–1848.

[4] Frazier, W. E., 2014. "Metal Additive Manufacturing: A Review". *Journal of Materials Engineering and Performance,* ***23***(6), Apr., pp. 1917–1928.



Copyright © 2017 ASME

Downloaded From: http://proceedings.asmedigitalcollection.asme.org/ on 11/07/2017 Terms of Use: http://www.asme.org/about-asme/terms-of-use

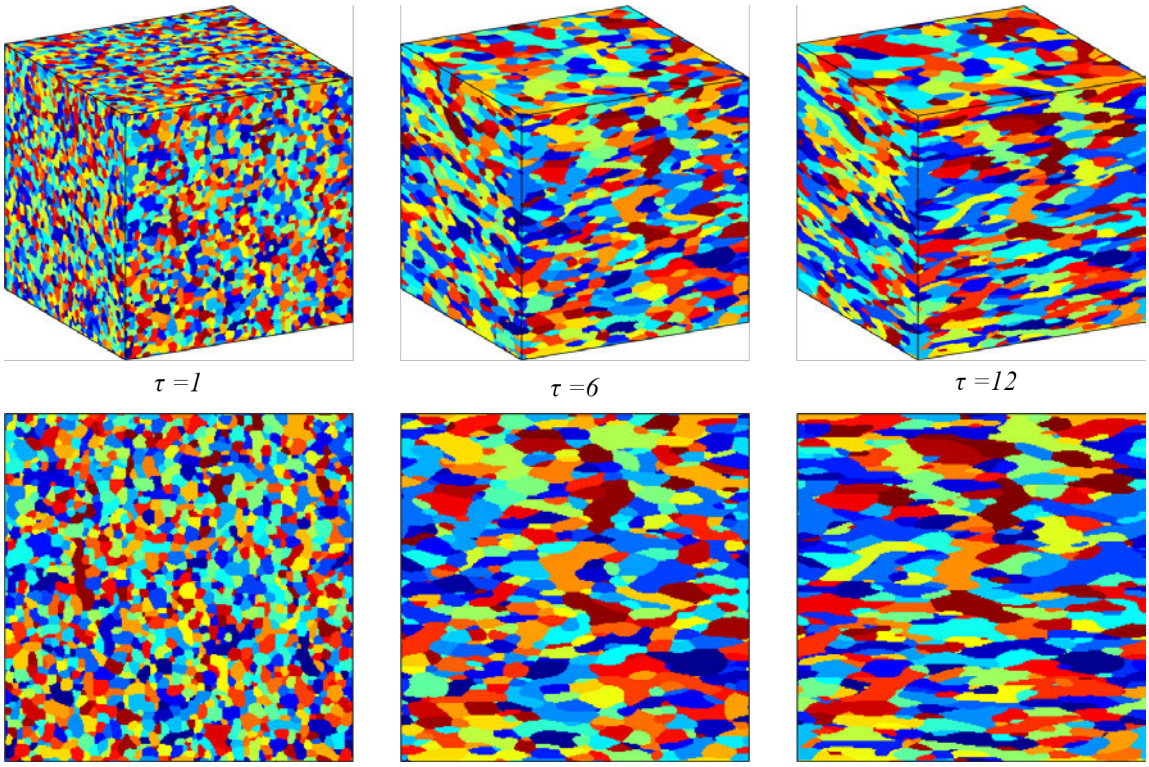


**FIGURE 2**: Simulated microstructures for $\tau = 1, 6, 12$ by the Continuous Diffuse-interface Method . 3D isometric views of a cubic RVE (top row), and respective front face views (bottom row) demonstrating the grain aspect ratio variability


[5] Song, B., Dong, S., Zhang, B., Liao, H., and Coddet, C., 2012. "Effects of processing parameters on microstructure and mechanical property of selective laser melted ti6al4v". *Materials & Design,* ***35***, pp. 120 – 125. New Rubber Materials, Test Methods and Processes.

[6] Simonelli, M., Tse, Y. Y., and Tuck, C., 2012. *Microstructure and Mechanical Properties of Ti-6A1-4V Fabricated by Selective Laser Melting*. John Wiley & Sons, Inc., pp. 863–870.

[7] Gu, D., Hagedorn, Y.-C., Meiners, W., Meng, G., Batista, R. J. S., Wissenbach, K., and Poprawe, R., 2012. "Densification behavior, microstructure evolution, and wear performance of selective laser melting processed commercially pure titanium". *Acta Materialia,* ***60***(9), pp. 3849 – 3860.

[8] Zhang, B., Liao, H., and Coddet, C., 2012. "Effects of processing parameters on properties of selective laser melting mg9*Materials & Design,* ***34***, pp. 753 – 758.

[9] Fonda, R., 2016. private communication.

[10] Boettinger, W. J., Warren, J. A., Beckermann, C., and Karma, A., 2002. "Phase-field simulation of solidification". *Annual Review of Materials Research,* ***32***(1), pp. 163–194.

[11] Fan, D., and Chen, L.-Q., 1997. "Computer simulation of grain growth using a continuum field model". *Acta Materialia,* ***45***(2), pp. 611 – 622.

[12] Waals, J. v., 1894. "van der: Arch. neerl. 28, 121 (1893); or". *Z. Phys. Chem,* ***13***, p. 657.

[13] Cahn, J. W., and Hilliard, J. E., 1958. "Free energy of a nonuniform system. I. interfacial free energy". *The Journal of Chemical Physics,* ***28***(2), pp. 258–267.

[14] Langer, J. S., 1986. *Directions in Condensed Matter Physics*. ch. Models of Pattern Formation in First-Order Phase Transitions, pp. 165–186.

[15] Karma, A., 2001. "Phase-field formulation for quantitative modeling of alloy solidification". *Phys. Rev. Lett.,* ***87***, Aug, p. 115701.

[16] Chen, L.-Q., 2002. "Phase-field models for microstructure evolution". *Annual Review of Materials Research,* ***32***(1), pp. 113–140.

[17] Thornton, K., gren, J., and Voorhees, P., 2003. "Modelling the evolution of phase boundaries in solids at the meso- and nano-scales". *Acta Materialia,* ***51***(19), pp. 5675 – 5710. The Golden Jubilee Issue. Selected topics in Materials Science and Engineering: Past, Present and Future.

[18] Moelans, N., Blanpain, B., and Wollants, P., 2008. "An introduction to phase-field modelling of microstructure evolution[j]". *Calphad*, pp. 268–294.



Copyright © 2017 ASME

**Downloaded From: http://proceedings.asmedigitalcollection.asme.org/ on 11/07/2017 Terms of Use: http://www.asme.org/about-asme/terms-of-use**

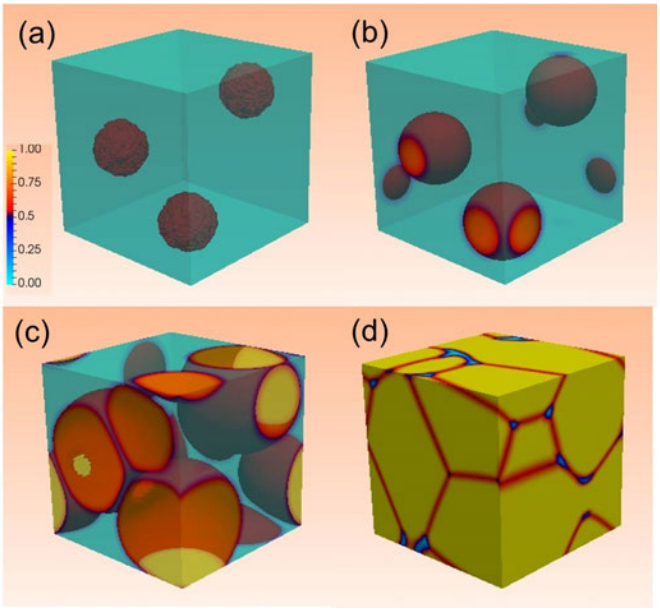


**FIGURE 3**: Simulated microstructures by the Multi Phase Field Method of 3-D Ni solidification of Ni at times: (a) 0 ps, (b) 100 ps, (c) 200 ps, and (d) 300 ps


[19] Kitashima, T., 2008. "Coupling of the phase-field and calphad methods for predicting multicomponent, solid-state phase transformations". *Philosophical Magazine,* ***88***(11), pp. 1615–1637.

[20] Jamshidian, M., and Rabczuk, T., 2014. "Phase field modelling of stressed grain growth: Analytical study and the effect of microstructural length scale". *J. Comput. Phys.,* ***261***, Mar., pp. 23–35.

[21] Areias, P., Msekh, M., and Rabczuk, T., 2016. "Damage and fracture algorithm using the screened poisson equation and local remeshing". *Engineering Fracture Mechanics,* ***158***, pp. 116 – 143.

[22] Amiri, F., Milln, D., Shen, Y., Rabczuk, T., and Arroyo, M., 2014. "Phase-field modeling of fracture in linear thin shells". *Theoretical and Applied Fracture Mechanics,* ***69***, pp. 102 – 109. Introducing the new features of Theoretical and Applied Fracture Mechanics through the scientific expertise of the Editorial Board.

[23] Vu-Bac, N., Bessa, M. A., Rabczuk, T., and Liu, W. K., 2015. "A multiscale model for the quasi-static thermoplastic behavior of highly cross-linked glassy polymers". *Macromolecules,* ***48***(18), pp. 6713–6723.

[24] Steinbach, I., and Pezzolla, F., 1999. "A generalized field method for multiphase transformations using interface fields". *Physica D: Nonlinear Phenomena,* ***134***(4), pp. 385 – 393.

[25] Eiken, J., Böttger, B., and Steinbach, I., 2006. "Multiphase-field approach for multicomponent alloys with extrapolation scheme for numerical application". *Phys. Rev. E,* ***73***, Jun, p. 066122.

[26] Steinbach, I., 2009. "Phase-field models in materials science". *Modelling and Simulation in Materials Science and Engineering,* ***17***(7), p. 073001.

[27] Hoyt, J. J., Asta, M., and Karma, A., 2001. "Method for computing the anisotropy of the solid-liquid interfacial free energy". *Phys. Rev. Lett.,* ***86***, Jun, pp. 5530–5533.

[28] Hoyt, J. J., and Asta, M., 2002. "Atomistic computation of liquid diffusivity, solid-liquid interfacial free energy, and kinetic coefficient in au and ag". *Phys. Rev. B,* ***65***, Jun, p. 214106.

[29] Asta, M., Hoyt, J. J., and Karma, A., 2002. "Calculation of alloy solid-liquid interfacial free energies from atomic-scale simulations". *Phys. Rev. B,* ***66***, Sep, p. 100101.

[30] Hoyt, J., Sadigh, B., Asta, M., and Foiles, S., 1999. "Kinetic phase field parameters for the cuni system derived from atomistic computations". *Acta Materialia,* ***47***(11), pp. 3181 – 3187.

[31] Bragard, J., Karma, A., Lee, Y. H., and Plapp, M., 2002. "Linking phase-field and atomistic simulations to model dendritic solidification in highly undercooled melts". *Interface Science,* ***10***(2), pp. 121–136.

[32] Sun, D. Y., Asta, M., and Hoyt, J. J., 2004. "Crystal-melt interfacial free energies and mobilities in fcc and bcc fe". *Phys. Rev. B,* ***69***, May, p. 174103.

[33] Danilov, D., Nestler, B., Guerdane, M., and Teichler, H., 2009. "Bridging the gap between molecular dynamics simulations and phase-field modelling: dynamics of a [ni x zr 1 x ] liquid zr crystal solidification front". *Journal of Physics D: Applied Physics,* ***42***(1), p. 015310.

[34] Guerdane, M., Wendler, F., Danilov, D., Teichler, H., and Nestler, B., 2010. "Crystal growth and melting in nizr alloy: Linking phase-field modeling to molecular dynamics simulations". *Phys. Rev. B,* ***81***, Jun, p. 224108.

[35] Fu, Y., Michopoulos, J. G., and Song, J.-H., 2016. "Bridging the multi phase-field and molecular dynamics models for the solidification of nano-crystals". *Journal of Computational Science*, p. in print.

[36] Yoon, Y.-C., and Song, J.-H., 2014. "Extended particle difference method for weak and strong discontinuity problems: part i. derivation of the extended particle derivative approximation for the representation of weak and strong discontinuities". *Computational Mechanics,* ***53***(6), pp. 1087–1103.

[37] Yoon, Y.-C., and Song, J.-H., 2014. "Extended particle difference method for weak and strong discontinuity problems: part ii. formulations and applications for various interfacial singularity problems". *Computational Mechanics,* ***53***(6), pp. 1105–1128.

[38] Yoon, Y.-C., and Song, J.-H., 2014. "Extended particle dif-



Copyright © 2017 ASME

Downloaded From: http://proceedings.asmedigitalcollection.asme.org/ on 11/07/2017 Terms of Use: http://www.asme.org/about-asme/terms-of-use

ference method for moving boundary problems". *Computational Mechanics,* ***54***(3), Sept., pp. 723–743.

[39] Hoyt, J. J., Asta, M., and Karma, A., 2001. "Method for computing the anisotropy of the solid-liquid interfacial free energy". *Phys. Rev. Lett.,* ***86***, Jun, pp. 5530–5533.

[40] Lechner, W., and Dellago, C., 2008. "Accurate determination of crystal structures based on averaged local bond order parameters". *The Journal of Chemical Physics,* ***129***(11), p. 114707.

[41] Nishida, Y., Aiga, F., and Itoh, S., 2014. "Microstructual path analysis of polycrystalline solidification by using multi-phase-field method incorporating a nucleation model". *Journal of Crystal Growth,* ***405***, pp. 110 – 121.

[42] Kim, S. G., Kim, D. I., Kim, W. T., and Park, Y. B., 2006. "Computer simulations of two-dimensional and three-dimensional ideal grain growth". *Phys. Rev. E,* ***74***, Dec, p. 061605.

[43] Achuthan, A., Iliopoulos, A. P., Michopoulos, J. G., Saunders, R., and Bagchi, A., 2017. "Towards a constitutive model that encapsulates microstructural features induced by powder additive manufacturing". In Proceedings of the ASME 2017 International Design Engineering Technical Conferences & Computers and Information in Engineering Conference IDETC/CIE 2017, ASME, p. Under Review.



Copyright © 2017 ASME

**Downloaded From: http://proceedings.asmedigitalcollection.asme.org/ on 11/07/2017 Terms of Use: http://www.asme.org/about-asme/terms-of-use**